Relativistic Motion Around Black Holes

Patrick Bush III

[1] San Diego State University, Department of Physics

Keywords: black hole, Schwardzschild, geodesics, test particle.

Abstract. In my project I explore the different possible orbits test particles may be subject to when orbiting a black hole (BH). The system is tested when the orbits are described by classical Newtonian gravitation, as well when derived from the general relativistic cases of a Schwarzschild metric. Comparisons between the precision and efficiency of the numerical integration methods of the Runge-Kutta 4th Order (RK4) and the Explicit Runge-Kutta method of order 5(4) (RK45) were also recorded for the two cases. Finally, the work was extended to incorporating the Kerr metric, which represents the spacetime due to a rotating BH.

1 Introduction

Black holes (BHs) are perhaps the most mysterious known objects in our universe. While they were surely theorized independently during the 18th century by the bright minds of John Michell and Pierre-Simon Laplace, it wasn't until 1915 when Albert Einstein concluded his theory of General Relativity (GR) that these object had mathematical truth to them. Ever since then, they have been a popular topic of research in astrophysics and astronomy alike. However, the dark and shrouded nature of BHs make them quite difficult to study directly.

Indirect observations of these objects must be made, and one of particular note is their gravitational influence they have on neighboring bodies. In the case of photons, we can see them fall into a BH and, in turn, illuminate a ring around it, giving it an identifiable outline. Additionally, the movement of surrounding stars could also provide information, in particular, quantities such as the mass of the BH.

In this project, I focus on modeling the orbital dynamics of bodies around BHs, using both Newtonian mechanics and general relativity. By simulating and comparing particle orbits in Schwarzschild spacetime to those governed by Newton's law of gravity, I explore relativistic phenomena like orbital precession, the existence of an innermost stable circular orbit (ISCO), and plunge behavior.

Observations of real systems like the S2 star orbiting Sgr A* — the SMBH at the center of the Milky Way — motivate this work. The relativistic corrections to its orbit are observable and help test GR in the strong-field regime.

To this end, a modular, object-oriented simulation package that integrates orbital motion through numerical methods was developed. Several single-particle orbit types were simulated and an extension that compares the behavior the test particles around a rotating BH versus the two previous spacetime descriptions. This allows us to explore how gravitational modeling choices affect the dynamics of bodies around a massive object.

2 Methods

2.1 *Physical Models*

The physical models used in this work are the Newtonian orbital motion and force law, as well as the Schwarzschild spacetime metric. In both cases, the geodesic equations that describe the motion of a test particle around a (static) BH are derived.

Although the Newtonian model may be familiar — as we will see in the next section — the Schwarzschild model may not. These geodesics are derived from the Schwarzschild metric, which is a solution to the Einstein field equations and corresponds to the external gravitational field of a static, spherically symmetric BH of mass M. The metric (with geometric units $G = c = 1$) is written as

$$ds^2 = (1 - \frac{2M}{r})dt^2 - (1 - \frac{2M}{r})^{-1}dr^2 - r^2 d\theta^2 - r^2 \sin^2\theta \, d\phi^2 \tag{1}$$

.

The derivation of the geodesic equations come from the Euler-Lagrange equations

$$\frac{d^2x^\mu}{d\tau^2} + \Gamma^\mu_{\alpha\beta}\frac{dx^\alpha}{d\tau}\frac{dx^\beta}{d\tau} = 0 \tag{2}$$

where the component derivatives are taken with respect to proper time $(d\tau)$ and the Christoffel symbols $(\Gamma^\mu_{\alpha\beta})$ are necessary. Due to the spherical symmetry of this spacetime, the test particle's motion is confined to the equatorial plane $(\theta = \frac{\pi}{2})$, which simplifies the geodesic equations.

2.2 *Governing Equations*

To set the groundwork for the two gravitational models, one must describe how one arrives at the necessary set of ordinary differential equations (ODEs). For both cases, the equations will be solved in polar coordinates — and later converted to Cartesian — since we will be plotting the orbits of test particles and would like to see how both the radial and angular components vary with time. In the Newtonian description, the process is started in [2], and the acceleration can be expressed as

$$\vec{a} = (\ddot{r} - r\dot{\phi}^2)\hat{r} + (r\ddot{\phi} + 2\dot{r}\dot{\phi})\hat{\phi} \tag{3}$$

.

Then consider the Newtonian gravitational force

$$\vec{F} = -\frac{GMm}{r^2}\hat{r} \tag{4}$$

.

Understanding $\vec{F} = m\vec{a}$ and then matching the radial and angular components of (3) and (4), one arrives at the set of second-order ODEs for the two components, namely

$$\ddot{r} = r\dot{\phi}^2 - \frac{GM}{r^2}, \quad \ddot{\phi} = -2\dot{r}\dot{\phi} \tag{5}$$

We will soon see how these along with their first-order reductions give the set of geodesic equations necessary to describe the motion of the test particles. The energy and angular momentum of the test particle in this model is given by

$$E = \frac{1}{2}v^2 - \frac{M}{r}, \quad L = vr, \tag{6}$$

where v is the orbital velocty of the particle.

For the Schwarzschild spacetime description, the derivation of the ODEs becomes more complex. The process will be skipped over here but [1] provides a detailed arrival at these equations:

$$\frac{dt}{d\tau} = \frac{E}{1 - 2M/r}, \qquad \frac{d^2r}{d\tau^2} = -\frac{M}{r^2} + \frac{L^2(r - 3M)}{r^4}, \qquad \frac{d\phi}{d\tau} = \frac{L}{r^2} \tag{7}$$

Here the conserved quantities of both the test particle energy (E) and angular momentum (L) are necessary inclusions. Notice also, the the derivatives are with respect to proper time $(d\tau)$ now, as mentioned in the previous section. The formulas of E and L for the circular orbit are

$$E = \sqrt{\frac{1-2M/r}{1-3M/r}}, \qquad L = \sqrt{\frac{Mr}{1-3M/r}} \tag{8}$$

The Schwarzschild effective potential is derived in detail in (EBH Book), but is essentially the second term in the radial geodesic equation $(\frac{dr}{d\tau})^2$, namely

$$V_{eff}(r) = (1 - \frac{2M}{r})(1 + \frac{L^2}{r^2}) \tag{9}$$

.

As we will see, the effective potential is a crucial quantity to track as it provides classification of the different type of Schwarzschild orbits when it is compared to the test particle energy.

2.3 *Numerical Methods*

The integration methods tested for the orbit simulations were the RK4 and RK45 methods, which only differed slightly as seen in the plots. RK45 was necessary for the Kerr orbits (Project Extension) since they offer time adaptive integration, however the resulting Kerr orbits surprisingly made more physical sense when RK4 was used.

In order to apply our chosen integration methods on the ODEs presented for each physical model, we must reduce the higher-order differential equations to first-order when necessary. The geodesics for the Newtonian case are as follows (in geometric units):

$$\frac{dr}{dt} = \dot{r}, \quad \frac{d\dot{r}}{dt} = r\dot{\phi}^2 - \frac{M}{r^2}, \quad \frac{d\phi}{dt} = \dot{\phi}, \quad \frac{d\dot{\phi}}{dt} = -2\dot{r}\frac{\dot{\phi}}{r} \tag{10}$$

.

Thus, the Newtonian state vector to track throughout the simulation is $[r, \dot{r}, \phi, \dot{\phi}]$. In a similar procedure, we arrive at the Schwarzschild geodesics:

$$\begin{aligned} \frac{dt}{d\tau} &= \frac{E}{1-2M/r}, & \frac{dr}{d\tau} &= \dot{r}, \\ \frac{d\dot{r}}{d\tau} &= -\frac{M}{r^2} + \frac{L^2(r-3M)}{r^4}, & \frac{d\phi}{d\tau} &= \frac{L}{r^2}, \end{aligned} \tag{11}$$

where the dotted quantities are now with respect to the proper time. The simplification of $(\theta = \frac{\pi}{2})$ makes the Schwarzschild state vector $[t, r, \dot{r}, \phi]$.

When modeling both the Newtonian and Schwarzschild orbits, the RK4 method was a rather appropriate one, as these systems were more or less smooth and well behaved. Additionally, it is faster per step compared to adaptive integration methods. The step size chosen was ultimately dependent on the starting radial value of the test particle — which differed with each orbital case — since it was computed from the period of the orbit and the number of steps. In each case, the step size was around 0.2, which was sufficient to capture the structure of the orbit visually.

The models were also tested using an adaptive method (RK45), in which most of the results were strikingly similar. It was only until the attempt at modeling the rotating BHs that this method was absolutely necessary, as it automatically adjusts the time step to control the local error, as well as performs better in handling stiff and chaotic systems.

3 Numerical Package Design

The makeup of the program developed includes the following: an object-oriented script including classes and the main executable function, a numerical methods module which held the integration techniques, and a module for the astrophysical constants used. The modularity of the object-oriented script in particular made it easy to extend this work to consider more complex spacetimes.

3.1 *Object-Oriented Structure*

In order to organize the different computational processes for each case's set of geodesics, a class for each (`NewtonGravity`, `SchwarzschildMetric`) was constructed. In addition to the geodesic method, the `SchwarzschildMetric` class also included an effective potential method, which was called when creating its plot to confirm each orbit outcome.

An `InitialConditions` class that included a method for each orbital case pertaining to its respective method was also developed. Namely, this would be: circular orbit for Newtonian model and circular, plunging, precessing orbits for Schwarzschild model. Within these methods is where the E and L were computed, along with the initial state vector components. Both the initial state and the conserved quantities were returned.

After the two classes, a few helper functions to add modularity that would be useful for my main executable function were put together. These included coordinate transformations (polar to cartesian), orbit classifications, initializations, and plotting/animation functions.

The executable function involved a main dictionary for orbit configurations for each case, and simulating the orbits for each case specified within the dictionary.

3.2 *ODE Solver and Physical Constants*

The classes in the numerical methods module that were used are the ODESolver and Integrator classes. As these were developed for past projects, both were revised in with extended modularity in order to plug in any geodesic function. The implementation of a generalized RK45 method also took place during this project, which meant consequently that the Integrator class needed additional revision to account for this method's adaptive nature.

A termination condition was also developed within the integrator. The reasoning behind this comes from the plunging orbit resulting in the particle shooting outwards after plunging into the BH. This condition made sure the simulation terminated once the particle reached the radii that constituted the event horizon $(R = 2M)$.

4 Execution Details

Parameters that were used throughout the GR equations were the BH mass M, test particle energy E, test particle angular momentum L, and the current radial value r. As for the integration of the different orbits, a step size was a necessary specification. The following process was used to arrive at this step size:

$$\text{steps} = 2000, \quad T_{\text{orbit}} = 2\pi\sqrt{\frac{r_0^3}{M}}, \quad T_{\text{total}} = 20 \cdot T_{\text{orbit}}, \quad \Delta t = \frac{T_{\text{total}}}{\text{steps}} \tag{12}$$

Note the increased orbital time compared to one orbital period. This was done to achieve the identifiable shapes of particular orbital cases, even though those such as circular and plunging orbits didn't require that many orbits.

As mentioned previously, the `Initial Conditions` class returned the initial state vector $[t, r, \dot{r}, \phi]$ and the conserved quantities $[E, L]$ for the Schwarzschild orbits, where the Schwarzschild Metric class returned the ODEs for the geodesics. This state vector and geodesic

function was passed into the ODE solver, then once integrated the time and state matrices were obtained.

The data structure that was constructed for each test particle consisted of each orbital case (1 Newtonian and 3 Schwarzschild) and their corresponding parameters. For the Newtonian model, the initial radius was $r_0 = 12M$ and the E and L was calculated accordingly. In the Schwarzschild model, the circular test particle orbit had $r_0 = 6M$ (ISCO), precessing orbit had $r_0 = 12M$, and the plunging orbit had $r_0 = 5.5M$.

A scaling factor was applied to the conserved quantities for the precessing case, such that its energy and angular momentum were

$$E_{precess} = \alpha E, \qquad L_{precess} = \beta L \tag{13}$$

where alpha was tried for different values until the it satisfied its corresponding effective potential relation. The values that obeyed these conditions were $\alpha = 0.92$, $\beta = 0.95$

For the plunging test particle, the simplest method for these quantities was used, namely assigning fixed values rather than computing it from the circular E and L. The values that resulted in the ideal behavior were $E = 1.05$ and $L = 3.0$.

Each case was looped through the integration process mentioned, and static plots as well as animated videos were obtained for each.

5 Results

For the test particle orbiting a BH while obeying the Newtonian equations of motion, the resulting orbit is circular as expected (Figure 1). The initial radial value of the particle was $r_0 = 12M$ and retained that distance throughout the orbital cycle.

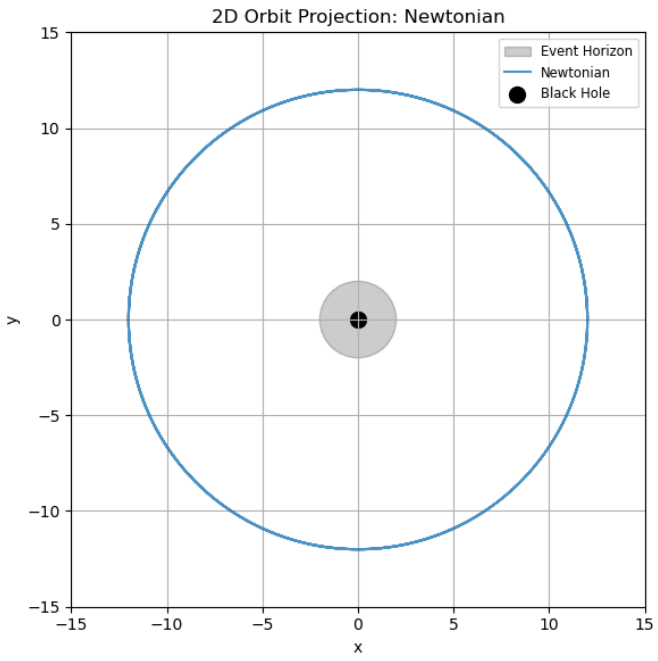

Figure 1: Orbit of a test particle governed by Newtonian gravity. The particle is initialized at radius $r = 12M$ with tangential velocity matching the circular orbital condition. The result is a perfectly circular trajectory, as expected for Newtonian two-body dynamics in the absence of perturbations.

When in GR using the Schwarzschild metric, the different orbital cases obey unique relations between the energy of the test particle and the effective potential curve that describes the system.

The relation for each case is

$$\begin{aligned} E^2 &= V_{\text{eff}}(r_0) && \text{(Circular orbit)} \\ \min V_{\text{eff}}(r) < E^2 &< \max V_{\text{eff}}(r) && \text{(Precessing orbit)} \\ E^2 &> V_{\text{eff}}(r) && \text{(Plunging orbit)} \end{aligned} \tag{14}$$

which were used to certify the orbit classifications (Figure 2).

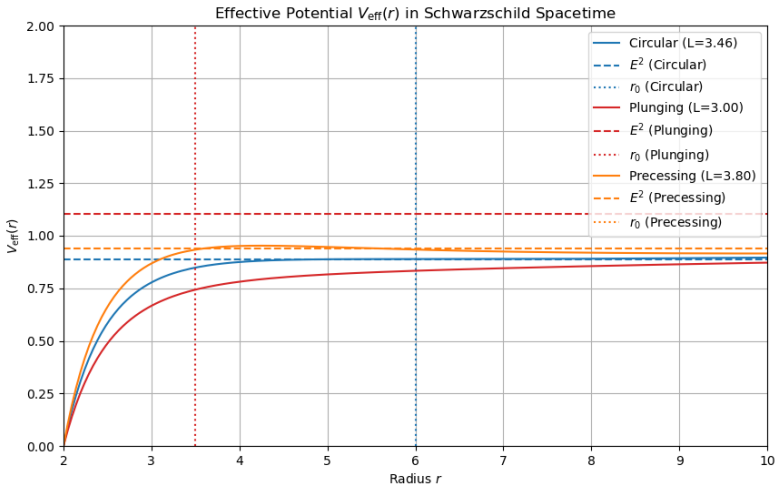

Figure 2: Effective potential $V_{\text{eff}}(r)$ for a test particle in Schwarzschild spacetime. The blue curve corresponds to a circular orbit where $E^2 = V_{\text{eff}}(r_0)$. The orange curve represents a bound, precessing orbit with energy between the potential's minimum and maximum. The red curve shows a plunging orbit with energy $E^2 > V_{\text{eff}}(r)$, allowing the particle to cross the event horizon. These distinctions illustrate how energy and effective potential together determine orbital behavior.

The different Schwarzschild orbits are shown in Figure 3(a)–(c), which all exhibit the desired orbital paths.

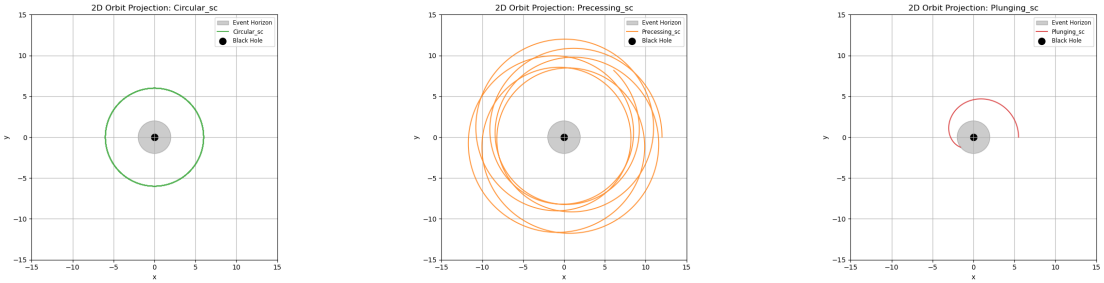

(a) Circular orbit (b) Precessing orbit (c) Plunging orbit

Figure 3: Simulated orbits of test particles in Schwarzschild spacetime. (a) A circular orbit occurs when the test particle's energy matches the effective potential at a specific radius. (b) A precessing orbit arises when the particle's energy lies between the potential minimum and maximum, resulting in bounded but non-repeating motion. (c) A plunging orbit occurs when the particle's energy exceeds the effective potential barrier, leading to infall into the black hole.

6 Analysis and Discussion

The resulting differences between the Newtonian Schwarzschild orbits are striking, and a display of the differences from the influence of relativistic effects. While the Newtonian orbit remained perfectly circular with a constant radial distance $r = 12M$, the Schwarzschild orbits showed several — relativistic-specific — distinct behaviors depending on the particle's energy and angular momentum.

The circular Schwarzschild orbit required a specific balance between energy and radius, and although visually similar to the Newtonian case, it exists only outside the ISCO ($R \geq 6M$). The precessing orbit was bound but not closed, exhibiting clear perihelion advance where the orbit slowly rotated around the BH with each revolution. The plunging orbit illustrated that when the particle's energy exceeds the effective potential maximum, no stable path exists to prevent a plunge into the event horizon ($r = 2M$) of the BH. This shift from bound motion to inevitable capture does not occur in Newtonian gravity.

Together, these plots explain the uniqueness of relativistic orbital dynamics and highlight features like the ISCO, orbital precession, and an event horizon plunge, all of which have no counterpart in Newtonian theory. The effective potential framework proved particularly valuable for predicting and interpreting these regimes, confirming the theoretical expectations of general relativity through numerical methods. Furthermore, these results emphasize that even when starting from similar initial conditions, a general relativistic model produces vastly different and more diverse orbital behavior than Newtonian gravity.

7 Project Extension: Kerr Metric Orbits

The extension I chose to implement in my project was an additional `KerrMetric` class, which models the motion of test particles around a rotating BH. Unlike the Schwarzschild metric, which assumes a non-rotating BH, the Kerr metric introduces frame-dragging effects due to the BH's angular momentum. These effects become especially important for orbits close to the event horizon and allow for phenomena such as the ergosphere and prograde/retrograde asymmetry.

The implementation required solving the full geodesic equations for the Kerr metric in Boyer–Lindquist coordinates. I generalized my integrator to handle 3D geodesics and circular equatorial orbits. Energy E, angular momentum L, and Carter's constant Q were the new set of constants of motion that defined initial conditions. For equatorial motion ($\theta = \pi/2,\ \ Q = 0$), the orbits successfully exhibited the expected relativistic effects, such as reduced ISCO (Figure 4).

However, the fully 3D non-equatorial Kerr simulations were not completely stable. Numerical errors accumulated rapidly in the θ-component of the geodesic equation, often leading to nonphysical behavior or failure to conserve conserved quantities. I attempted to stabilize the solver through clamping, bounding θ away from the poles, and modifying the effective potential terms, but the integration still became unreliable for long timescales. With theta clamped, the resulted plot can be found in the appendix.

Despite these limitations, the equatorial Kerr simulations clearly illustrated the departure from Schwarzschild dynamics and demonstrated the strong influence of spin on orbital structure. Full 3D Kerr simulations remain a promising direction for future work, especially with more advanced numerical techniques.

This extension highlights the power and challenge of relativistic modeling: even with idealized test particles, BH spin introduces qualitatively new physics that demands both theoretical care and numerical precision.

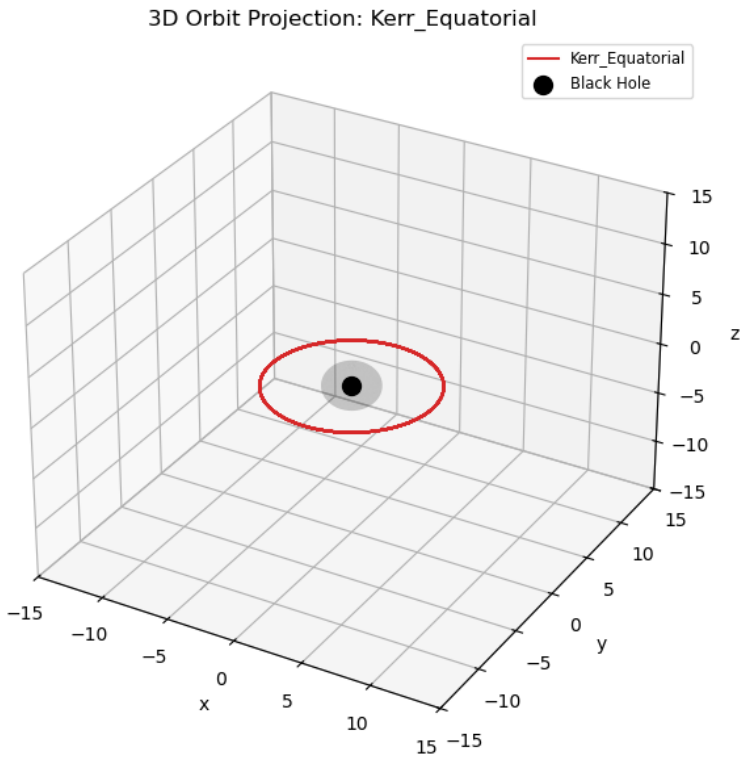

Figure 4: Test particle orbit in the Kerr equatorial spacetime. Relativistic effects from BH rotation allow for closer radii ($r = 4M$) than Schwarzschild spacetime allows.

8 Conclusion

In this project, I implemented and analyzed the motion of test particles under both Newtonian gravity and general relativity. Using custom ODE solvers and numerical integrators (RK4 and RK45), I simulated particle trajectories in Newtonian, Schwarzschild, and Kerr spacetimes. The results clearly demonstrate how general relativity produces qualitatively different orbital behavior — such as perihelion precession, the existence of unstable orbits, and eventual plunge into the BH event horizon — all nonexistent in Newtonian mechanics.

The effective potential framework I applied was especially valuable for classifying orbit types and connecting physical intuition to numerical results. Each relativistic orbit was verified by checking energy conditions against the potential curve, helping to reinforce the interpretation of conserved quantities in curved spacetime.

As an extension to my project, I implemented the Kerr metric to explore how BH spin influences orbital dynamics. While 3D Kerr orbits introduced numerical challenges, the equatorial orbits worked well. This highlighted both the power and difficulty of modeling rotating spacetimes.

Overall, this project illustrates how numerical methods can bring general relativity to life. Simulating particle motion in curved spacetime not only deepens understanding of relativistic physics but also offers a field for progressing numerical solvers for use in challenging dynamical systems.

9 Appendix

The following figures include supplemental visualizations from the extended simulations.

Figure 5 shows a 3D test particle orbit in Kerr spacetime with nonzero Carter constant Q, leading to inclined motion. Due to instabilities near the poles, the simulation required clamping in θ, limiting the orbit's physical realism over long timescales. This clamping fixed the iniital

problem where the ”orbit” just appeared as a red screen, however now the 3D Kerr orbit is just an arc.

Figure 6 displays a multi-particle Schwarzschild simulation. While this is not a true N-body simulation with mutual interactions, each test particle follows an independent relativistic geodesic corresponding to one of the key orbital types: circular, precessing, plunging, or escaping. It is worth noting that although the escaping orbit wasn't focused in this study, it was observed here. This is yet another case of an unstable orbit, where the E of the test particle is too large to remain in orbit.

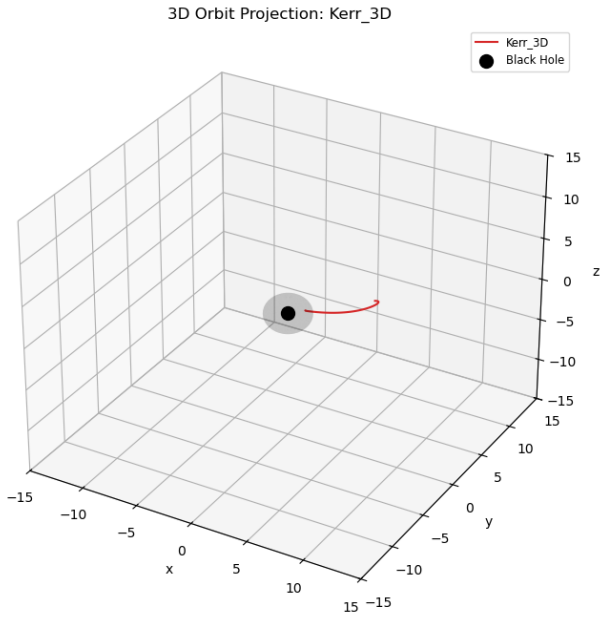

Figure 5: 3D inclined Kerr orbit with nonzero Carter constant.

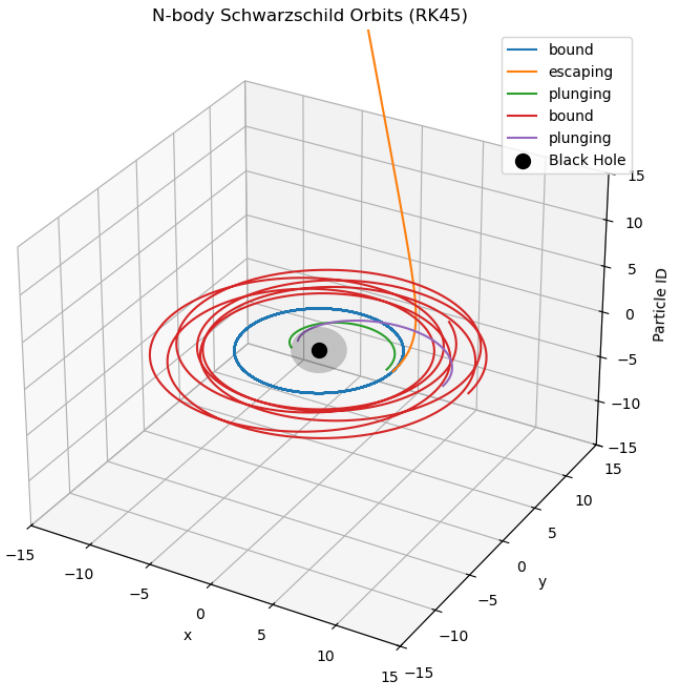

Figure 6: Simulated Schwarzschild orbits of five test particles.

References

[1] Carroll, S. (1997). *Lecture Notes on General Relativity*. arXiv:gr-qc/9712019.

[2] Taylor, J. R. (2005). *Classical Mechanics*. University Science Books.

[3] Taylor, E. F., & Wheeler, J. A. (2000). *Exploring Black Holes: Introduction to General Relativity*. Addison Wesley.

[4] Thorne, K. S. (1994). *Black Holes and Time Warps: Einstein's Outrageous Legacy*. W. W. Norton & Company.

[5] Sperhake, U. (2016). *Introduction to Numerical Relativity*. COST NewCompStar School Slides, University of Cambridge.

[6] Hopper, S., & Cardoso, V. (2016). *Numerical Relativity: (Almost) All You Need to Know*. Lecture notes, CERN.

[7] Press, W. H., Teukolsky, S. A., Vetterling, W. T., & Flannery, B. P. (2007). *Numerical Recipes: The Art of Scientific Computing* (3rd ed.). Cambridge University Press.

[8] *Schwarzschild Geodesics*. Wikipedia. https://en.wikipedia.org/wiki/Schwarzschild_geodesics

[9] *Kerr Metric*. Wikipedia. https://en.wikipedia.org/wiki/Kerr_metric